

Development of a novel method for Cu(II) sorption from aqueous solution and modeling by artificial neural networks (ANN)

Dorna Sobhani, Hassan Pahlavanzadeh*, Mohammad Sheiback

Faculty of Chemical Engineering, Tarbiat Modares University, Tehran, Iran, email: dorna.sobhani@gmail.com (D. Sobhani), pahlavzh@modares.ac.ir (H. Pahlavanzadeh), msheiback2005@outlook.com (M. Sheiback)

Received 10 November 2017; Accepted 24 March 2018

ABSTRACT

In this study, coal Fly Ash (FA) was used as a low-cost source of Si and Al to synthesize the Zeolite A (ZA) via a hydrothermal reaction. ZA and FA were characterized by XRD, XRF and SEM/EDX. A series of batch sorption experiments was carried out for the sorption of Cu(II) from aqueous solutions on ZA and FA. The obtained data revealed that maximum removal efficiencies were ~ 98% (with 0.3 g, 5 min, 5 of adsorbent dose, contact time and pH respectively for ZA) and 96% (with 0.3 g, 4 h, 5 of adsorbent dose, contact time and pH respectively for FA). Studying the kinetic of Cu(II) adsorption onto FA indicated the adsorption process was controlled by pseudo-second-order and intra-particle diffusion models. Isotherm models subjected to experimental data at $T = 25^{\circ}\text{C}$ demonstrated that Cu(II) adsorption onto ZA and FA were both favorable with good adsorption characteristics with maximum sorption capacity of 54.9 and 16.6 mg g^{-1} for ZA and FA respectively. The calculated amounts of thermodynamic parameters such as ΔH° , ΔS° and ΔG° showed that the adsorption of Cu(II) onto both FA and ZA was feasible, spontaneous and endothermic. Moreover, a three-layer artificial neural network was constructed to model the experimental data by matlab software. Levenberg–Marquardt back-propagation training function with 6 neurons in the hidden layer was found to be the most proper network.

Keywords: Coal fly ash; Zeolite; Adsorption; Cu(II); ANN

1. Introduction

Water, the most vital natural resource, is highly affected by daily disposal of heavy metals from diverse industries [1]. The wastewater or water with heavy metal ions brings about serious environmental risks, because these pollutants are highly toxic, persistent and non-biodegradable and tend to be accumulated in living organisms causing several health effects [2]. For instance, the presence of copper (standard limit of copper concentration is 0.2 mg L^{-1}) in water can cause vomiting, diarrhea, stomach cramps, nausea, greenish or bluish stools, hypotension, heart disease, premenstrual tension, postpartum depression, paranoid and hallucinatory schizophrenias, childhood hyperactivity and autism and may have severe effect in the brain and liver of people with Wilson's disease [3]. The human body has complex homeo-

static mechanisms which attempt to ensure a constant supply of available copper, while eliminating excess copper whenever this occurs. However, like all essential elements and nutrients, too much or too little nutritional ingestion of copper can result in a corresponding condition of copper excess or deficiency in the body, each of which has its own unique set of adverse health effects [4]. Cu(II) is produced by metallurgical, plating, printing circuits and mining activities and can be categorized as one of the most common heavy metal ions existing in industrial wastes [5].

Numerous techniques, such as chemical precipitation, electrocoagulation [6–8], reverse osmosis and membrane processes [9], ion exchange [10,11], and adsorption [12,13] have been widely applied for the removal of heavy metal ions from water and wastewater. Among these methods, adsorption seems to be the most attractive due to its high efficiency, fairly low cost, simplicity and easy handling, availability of a wide range of adsorbents as well as the

*Corresponding author.

possibility to operate at ambient temperature/pressure [14]. In recent years, the utilization of natural materials and industrial wastes such as human hair [15], natural/agricultural wastes biomass [16], sawdust [17], eggshell and coral wastes [18], waste crab shells [19], soil, coal fly ash [20,21], charcoal ash [22], lignin and natural zeolites [11], ostrich bone waste [23], etc. as low-cost adsorbents for wastewater treatment has been widely investigated.

Coal fly ash, the most abundant inorganic residue obtained from thermal power plants, has been known as a potential material for wastewater treatment due to its chemical composition, low cost and considerable adsorption properties [24,25]. The major components in fly ash, namely alumina and silica, has made it a potential precursor in synthesis of various types of zeolites which are porous aluminosilicate compounds having attractive characteristics such as molecular sieving, high thermal stability, ion exchange capability and shape selective catalytic behavior due to their special structures [24]. Approximately 24 types of different zeolites have been synthesized from coal fly ash; among them, zeolite A and X have more attractive properties, especially in wastewater decontamination processes because of their high CEC resulted from their low Si/Al ratio as well as their large pores [24,26]. On the other hand, there are few studies in literature regarding the adsorption of Cu(II) on zeolite A as an attractive adsorbent.

Artificial neural network (ANN) represents a non-traditional processing system based on the human brain's biological network in problem solving processes [27]. ANNs are composed of multiple interconnected non-linear processing elements operating in parallel which determine the network output based on the available experimental information [28]. In recent years, ANNs have attracted significant attentions due to their prominent advantages over the conventional computational systems including the capacity of producing complex and transparent mappings, simplicity and adaptability, robustness, fault tolerance and also not requiring the complex nature of the underlying process [5,29–32].

In the present work, pure zeolite A was synthesized through a two-step process (alkaline fusion - hydrothermal synthesis) using raw coal fly ash and characterized using XRD and SEM/EDX. The prepared zeolite as well as the raw material (coal fly ash) were used as adsorbents for the removal of copper ions from aqueous solution. The effect of various operational parameters, such as initial pH, initial Cu(II) concentration, adsorbent dosage, contact time and temperature on the removal of Cu(II) was investigated. ANN modeling approach was applied to predict Cu(II) removal efficiency of the prepared zeolite and the raw fly ash as well. Finally, output results obtained from the model were compared with the experimental data. In addition, in order to better understanding of the adsorption characteristics, isotherm, kinetic and thermodynamic models were also studied.

2. Materials and methods

2.1. Materials

Raw coal fly ash was collected from a combustion test furnace in Alborzsharghi Coal Company which is located in

Sharood (Iran). Stock copper solution with 1000 mg L^{-1} concentration was prepared by dissolving 3.8 g of its nitrate salt ($\text{Cu}(\text{NO}_3)_2 \cdot 3\text{H}_2\text{O}$) in 1 L of distilled water. The copper solutions with the required concentrations were freshly made by serial dilution of the stock solution with distilled water. To adjust the pH of the solution, 0.1–1.0 M HNO_3 and 0.1–1.0 M NaOH solutions were used. Sodium hydroxide (97%) and sodium aluminate (99.99%) utilized for zeolite synthesizing and all other chemicals used throughout this study were purchased by Merck.

2.2. Zeolite synthesis

A two-step process was taken to synthesize pure zeolite A [26]. Typically, raw coal fly ash was mixed with solid NaOH in mass ratio of 1:1.2. The mixture was heated at 823 K for one hour. After the alkaline fusion step, the mixture was cooled at room temperature and milled into fine powders. Calculated amount of sodium aluminate was added to the grinded mixture to control the molar ratio of $\text{SiO}_2/\text{Al}_2\text{O}_3$ and mixed with water. The mixture was then stirred at room temperature at the speed of 400 rpm for 16 h. At this time, the slurry was sealed in a Teflon-lined autoclave and heated to 373 K in an oven for hydrothermal synthesis for 7 h. After cooling down to room temperature, the suspension was filtered and the solid was washed several times with deionized water and dried at 378 K for 16 h. Finally, the synthesized zeolite was characterized and used in the sorption experiments.

2.3. Characterization of adsorbents

The elemental characterization of the coal fly ash was carried out on PHILIPS PW2404 X-ray fluorescence (XRF) spectrophotometer. The mineralogical compositions of raw fly ash (FA) and the zeolite prepared from it (ZA) were determined by a GBC X-ray Diffractometer using Cu K α radiation at 35 kV and 28.5 mA. The scan was continuous with the step time of 0.5 s, in a range of 10–60 (2θ). Surface morphology of the adsorbents was analyzed by scanning electronic microscopy coupled with EDX analysis (SEM/EDX, HITACHI, S-4160, Japan). In the SEM analysis, the adsorbent samples were covered with a thin layer of gold and mounted on a copper stub using a double-stick tape.

2.4. Batch adsorption experiments

The adsorption of copper ions from aqueous solution onto raw fly ash and the zeolite prepared from it was done in a batch mode using a magnetic stirrer (Heidolph MR 3001K). Experiments to determine the optimum pH were carried out at room temperature (25°C) by adding 0.3 g of adsorbent into 50 ml of Cu(II) solution with the concentration of 50 mg L^{-1} at various pH values ranging from 2 to 6 and each sample was stirred at 400 rpm for 6 hours. To determine the effect of contact time on Cu(II) adsorption onto FA at the optimum pH determined in the previous step, samples were taken at specified time intervals of 0.5-1-2-3-4-5-6 h. Also, contact times of 5, 10, 20, 30 and 60 min were studied for Cu(II) adsorption onto ZA. Experiments to investigate the effect of adsorbent dosage were

performed at 25°C by adding different adsorbent dosages ranging from 0.05 to 0.4 g into 50 ml of Cu(II) solution (50 mg L⁻¹) with the optimum pH and contact time obtained in the previous steps. Experiments to study the effect of initial Cu(II) concentration were carried out by adding the optimum adsorbent dosage in 50 ml of Cu(II) solution. The initial pH of solutions and contact times were also optimized. Various initial Cu(II) concentrations ranging from 50 to 250 mg L⁻¹ were chosen. Tests to determine the optimum temperature in Cu(II) adsorption onto FA and ZA were accomplished at three different temperatures of 25, 35 and 45°C by adding the optimum adsorbent dosage in 50 ml of Cu(II) solution with the concentration of 50 mg L⁻¹. After predetermined intervals in each experiment, the suspension of the adsorbent was separated from solution by filtration and the filtrate was analyzed to measure the final Cu(II) concentration using an atomic adsorption spectrophotometer (AAS, Varian, model AA240). All the experiments were repeated twice to minimize the experimental error (below 4%), and the average data was reported. The removal efficiency of Cu(II), %Removal, was calculated according to the following equation:

$$\%Removal = \frac{C_i - C_f}{C_i} \times 100 \quad (1)$$

where C_i (mg L⁻¹) and C_f (mg L⁻¹) are the initial and final concentration of Cu(II) in the solution respectively. q (mg g⁻¹) is the amount of metal ion adsorbed per mass unit of adsorbent. The adsorption capacity at time t , q_t (mg g⁻¹) can be obtained by the following equation:

$$q_t = (C_i - C_t) \times \frac{V}{m} \quad (2)$$

where C_t (mg L⁻¹) is Cu(II) concentration at any time t ; V (L) is the solution volume and m (g) is the mass of adsorbent.

The amount of adsorption at equilibrium, q_e (mg g⁻¹) is given by:

$$q_e = (C_i - C_e) \times \frac{V}{m} \quad (3)$$

where C_e (mg L⁻¹) is the copper ion concentration at equilibrium.

2.5. Artificial neural network modeling

Artificial neural networks, powerful models simulating analytical functions of the human brain, use experience and experiment to learn and identify complex and highly non-linear multivariable systems. The ability to extract the desired outputs using the experimental input data, without the need for additional experiments, as well as their reliability and capacity in terms of capturing nonlinear relationships between variables in complex systems has made ANNs efficient and powerful modeling techniques applied in many scientific applications and industrial processes including the prediction of adsorption systems [33,34]. Artificial neurons, fundamental processing units in ANNs, are located in three types of layers: one input layer which contains neurons representing independent variables, one output layer in which neurons representing dependent variables exist, and multiple hidden layers [35]. In the

ANN structure, each neuron is connected to other neurons existing in the neighbor layer. The interconnection pattern among the neurons is called the network architecture. There are several ANN architectures applied in engineering applications, among which the Multi-layer Perceptron (MLP) is an extensively used feed forward network architecture which uses back-propagation (BP) learning algorithm [34]. In the feed-forward neural networks, information moves only in the forward direction from the input to the hidden and finally to the output layer [33].

In the MLP network, each connecting line corresponds to a certain weight. The network training is implemented by adjusting these weights leading to minimize the network error function. As presented in Eq. (4), applying a transfer function to a weighted summation of its inputs results in a neuron output which in turn serves as input to other neurons [34]:

$$\gamma_{jk} = F_k \left(\sum_{i=1}^{N_{k-1}} W_{ijk} \gamma_{i(k-1)} + \beta_{jk} \right) \quad (4)$$

where β_{jk} is the bias weight for neuron j in layer k and γ_{jk} is the neuron j 's output from k 's layer. The model-fitting parameters (W_{ijk}) are the connection weights that were selected randomly and F_k is the nonlinear activation transfer function that may appear in various forms including Identity function, Binary step function, Binary sigmoid, Bipolar sigmoid, Gaussian as well as linear functions [36].

In this study, we applied a three-layer feed-forward MLP network using Levenberg-Marquardt back-propagation training function to predict the adsorption process of Cu(II) from aqueous solution. Fig. 1 shows the MLP network used in this work consisting of one input layer with 5 neurons (pH, contact time, adsorbent dosage, initial Cu(II) concentration, and temperature), one output layer with 1 neuron (% removal efficiency), and one hidden layer with 6 neurons. In order to evaluate the integrity of the experimental data fit and the prediction accuracy of the model and to choose the best network architecture, the mean square error (MSE) was calculated according to the following equations [33,36]:

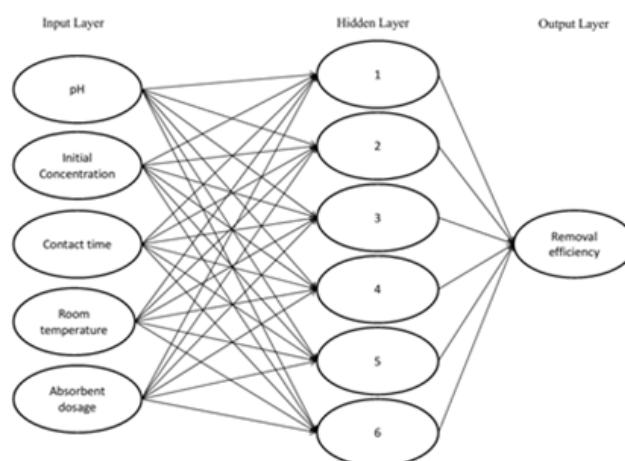


Fig. 1. Schematic diagram of the neural network structure for Cu(II) removal.

$$MSE = \frac{\sum_{i=1}^n (y_i - \hat{y}_i)^2}{n} \quad (5)$$

where y_i , \hat{y}_i and n are experimental data, predicted data, and the number of experiments, respectively. The neural network was examined with different number of neurons to identify the optimum number of neurons in the hidden layer by obtaining the minimum MSE. Results of prediction by neural network (mean square error) for different transfer function are presented in Table 1.

3. Results and discussion

3.1. Characterization of adsorbents

Table 2 indicates the chemical composition of raw fly ash as determined by XRF. It is obvious that the main elements include O, Si, Al, Fe, Ca, and Mg as well as trace amounts of K, Na, S and Li. By 84.68% of total Fe_2O_3 , Al_2O_3 and SiO_2 compounds, the used fly ash can be categorized as Class F fly ash in terms of ASTM C618-99 specification.

The X-ray diffraction (XRD) spectrums of FA and ZA are shown in Fig. 2. As it is observed, diffraction peaks of Quartz (SiO_2), Hematite (Fe_2O_3), Anhydrite ($CaSO_4$), Magnetite (Fe_3O_4) and Lime (CaO) are found in the XRD pattern

Table 1
Results of artificial neural network for prediction of adsorption amounts

Transfer function	Number of neurons	MSE (mean Square Error)	
		FA	ZA
Logsig	4	3.01	1.91
Logsig(n) = $\frac{1}{1+e^{-n}}$	6	1.10	0.139
	10	1.79	0.44
Tansig	4	6.11	0.400
a = $\frac{2}{1+e^{-2n}} - 1$	6	1.48	0.38
	10	3.66	0.93
Linear a = n	4	2.20	1.96
	6	1.18	2.07
	10	4.73	6.19

Table 2
Chemical composition of raw fly ash by XRF

Component	% mass
LiO	0.98
SiO_2	37.88
Al_2O_3	28.73
Fe_2O_3	18.07
CaO	11.54
MgO	1.79
SO_3	0.38
K_2O	0.34
Na_2O	0.29

of raw fly ash, with quartz being the main crystalline phase. Although the composition of Al_2O_3 in the raw fly ash is near 28% (Table 2), aluminum mineralogical phases such as mullite could not be found in the XRD pattern of FA. That is probably due to the fact that the minerals present in the coal dictates the elemental composition of the fly ash, while the mineralogy and crystallinity of the ash is dictated by the boiler design and operation [37]. The XRD pattern of ZA can also be seen in Fig. 2. According to the diffractogram, the synthesized product presents the pure phase of zeolite A.

The surface morphologies of FA and ZA are shown in Figs. 3a–d. As can be seen in the images of FA, fly ash particles are generally spherical and irregular in shape, in accordance with literature [38,39]. In addition, a smooth surface and fairly nonporous structure can be observed for the ash. Actually, diverse physical states of silica existing in fly ash are responsible for the particles of irregular sizes [38]. Figs. 3b,d illustrate morphology changes of ZA. According to literature, zeolite A presents a cubic structure. The structure of zeolite A is fitted in by a β -cage (the fundamental structure of sodalite) interconnected with double 4-ring units (D4R) [40]. The SEM micrographs confirm the presence of pure zeolite A. Furthermore, the surface morphology and chemical structure of the zeolite was analyzed using SEM/EDX after adsorption. The results are shown in Fig. 4. As can be observed, the cubical structure of the zeolite did not change during the adsorption process and the small particles attached to zeolite may assume to be Cu(II) adsorbed onto the zeolite surface. In addition, the EDX analysis confirms the adsorption of copper ions onto zeolite since the peak of Cu atom is seen in the EDX analysis while there was no Cu atom in the chemical composition of raw fly ash (Table 2) and consequently the zeolite prepared from it.

3.2. Effect of initial solution pH

The aqueous solution pH is a vital parameter controlling the adsorption process of metal ions from aqueous solution as it can affect the surface charge of adsorbent, the chemical speciation of metal ions as well as the ionization of the functional groups on the adsorbent surface [41,42]. For the purpose of investigating the influence of initial solution pH on the adsorption of copper ions onto FA and ZA, the batch adsorption experiments were accomplished in pH range of 2

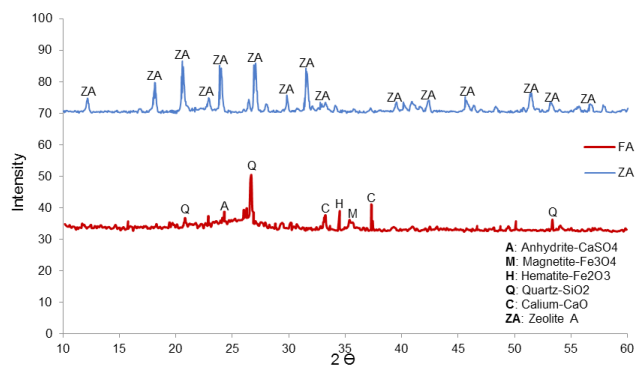


Fig. 2. X-ray diffraction patterns of FA and ZA.

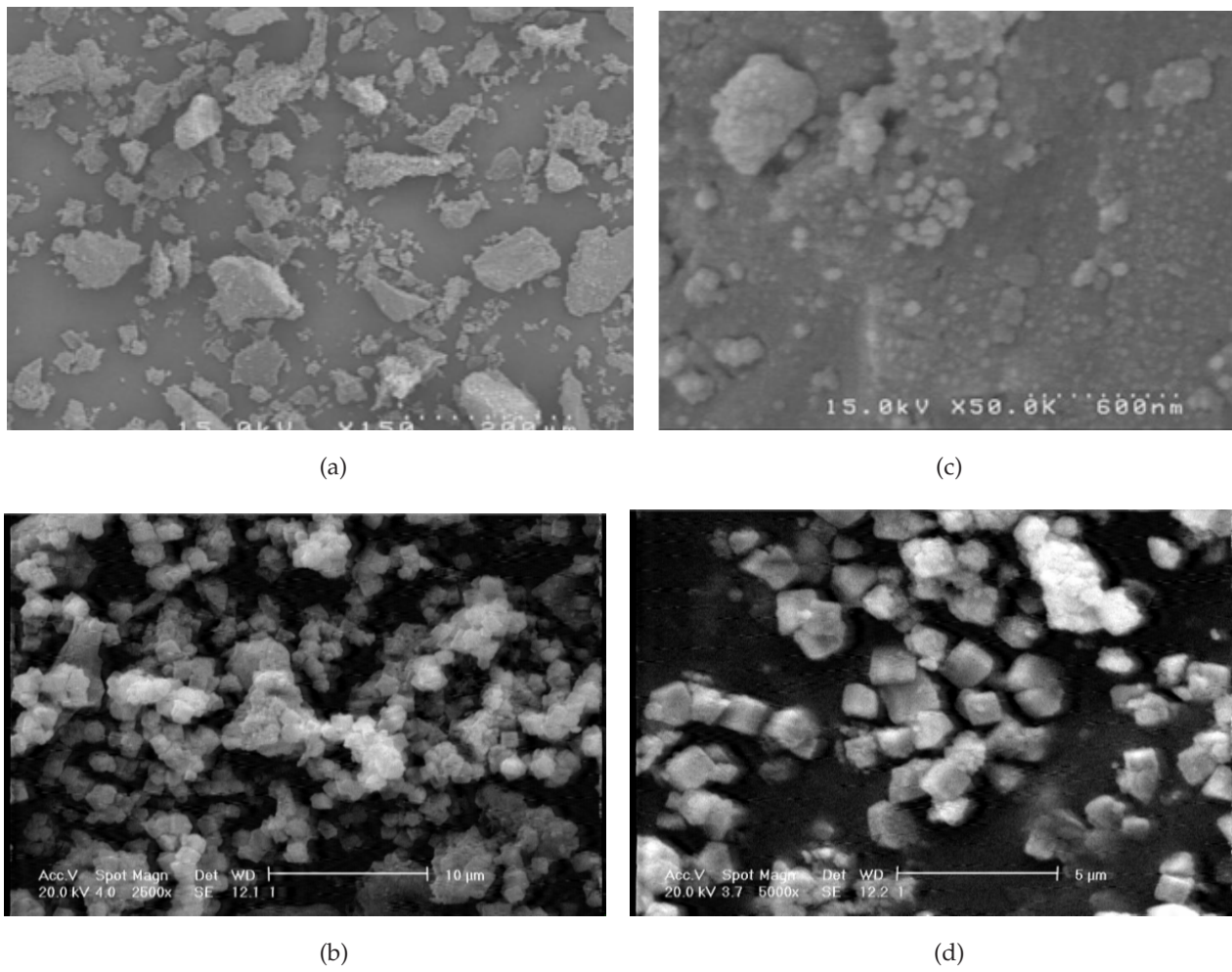


Fig. 3. SEM images of (a) FA, (b) ZA, (c) FA with more zoom, (d) ZA with more zoom.

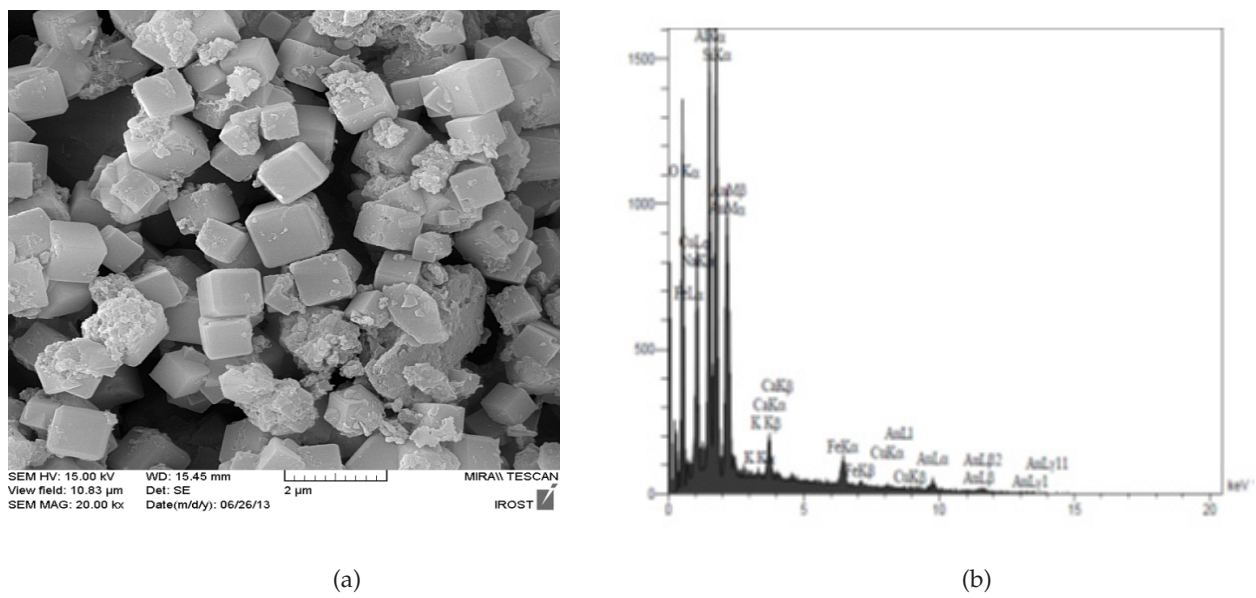


Fig. 4. SEM image and EDX analysis of ZA after adsorption.

to 6, avoiding the precipitation of insoluble Cu(II) hydroxides formed at pH values higher than 6 [21]. The obtained results are presented in Fig. 5. As it is observed, the removal efficiency of Cu(II) increased with the increase of pH. It means that both FA and ZA have higher performances for Cu(II) removal in weak acidic or neutral solution than that in strong acidic media. Lower adsorption capacities observed for copper ions at pH values below 4 can be attributed to more existing hydrogen ions which strongly compete with metal ions for the same negatively charged adsorption sites on the adsorbent surface. Besides, the electrostatic repulsion of H⁺ ions prevents the approach of metal ions to the adsorbent surface at low pH values. In addition, under strong acidic conditions, the H⁺ ions in the solution can neutralize the basic anhydride on the surface of the adsorbent, diminishing the adsorption capacity [39]. As the pH increases, the concentration of H⁺ ions in the solution decreases which leads to an increase in the amount of adsorbed metal ions. The mechanism of removing divalent metal ions including Cu(II) at high pH values can be assumed to be a combination of adsorption and precipitation processes [5,39]. The optimum pH for copper adsorption onto both FA and ZA was determined to be 5, in which the maximum removal efficiency of 96.5% has been achieved for FA, whereas the adsorption efficiency of copper ions onto ZA was in a higher range (81.1–98.9%). Furthermore, another advantage of ZA over FA to be used as an adsorbent for Cu(II) removal is to achieve high removal efficiencies in a wide range of pH (3–6). The main adsorption mechanism in cation removal by zeolites is ion exchange with exchangeable cations in the structure of the zeolite such as Ca²⁺, Mg²⁺, K⁺ and Na⁺. Cation exchange capacity (CEC) of these materials can be measured by the number of negatively charged sites attracting exchangeable cations. The negative charge resulted from the substitutions within the lattice structure is enduring and does not depend on pH, while the charges on the edges and the exposed hydroxyls surface are pH dependent [43].

3.3. Effect of contact time

The effect of contact time on the adsorption of Cu(II) from aqueous solution onto FA and ZA is depicted in Figs. 6a,b. The results show that the removal efficiency of copper ions by FA increased with the increase of contact

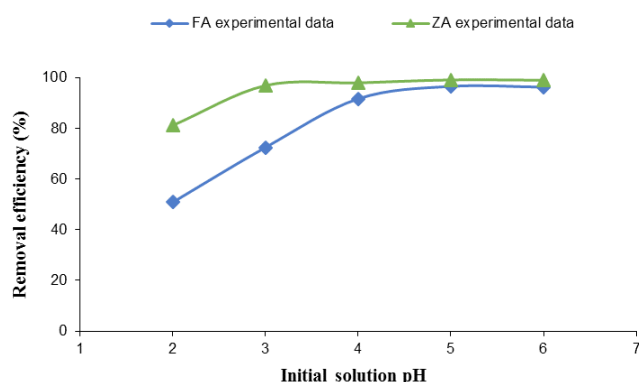
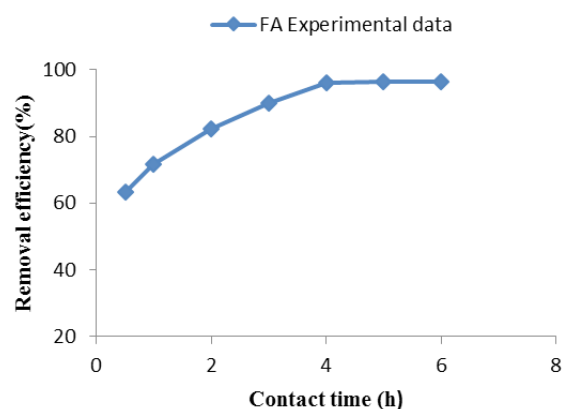
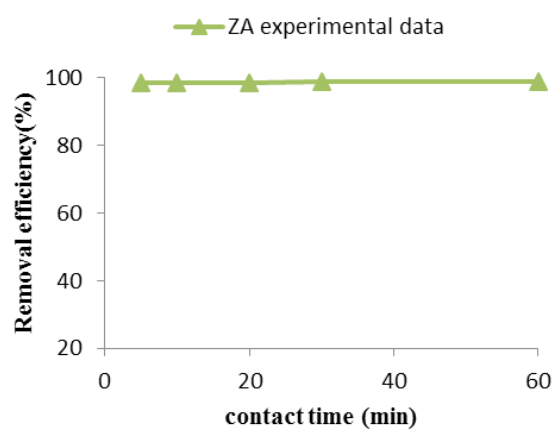


Fig. 5. Experimental data for pH effect on the removal efficiency of Cu(II) by FA and ZA.

time until the adsorption process attained an equilibrium state after approximately 5 h. In other words, the adsorption efficiency of Cu(II) onto FA increased to 63.4% at 30 min. As can be seen, longer time is required for the removal of Cu(II), i.e., 96.4% of Cu(II) is adsorbed after 4 h. The relatively fast adsorption rate within the first hours before the equilibrium time was probably due to the abundant availability of vacant active sites for the metal ions to adsorb on. Further increase in contact time after the equilibrium time did not have significant influence on the adsorption percentage since almost all active sites on the adsorbent surface were occupied and also there was a repulsive force between the adsorbed molecules and their homologues in the bulk phase [44,45]. In addition, based on Fig. 6b, it is evident that the adsorption efficiency of copper ions onto ZA also increases slightly with the increase of contact time. Since the amount of adsorbed Cu(II) onto ZA did not significantly change with time, the minimum contact time of 5 min with the removal efficiency of 98.4% was set as the optimum adsorption time for the later experiments. The fast ion uptake by the synthesized zeolite used in the experiments may be attributed to its highly porous structure which provides a large surface area with far more active adsorption sites for the adsorbates. It should be noted that by utilizing ZA instead of FA in adsorp-



(a)



(b)

Fig. 6. Experimental data for contact time effect on the removal efficiency of Cu(II) by (a) FA and (b) ZA.

tion of Cu(II), high removal efficiencies can be achieved in far less time, making ZA a highly attractive adsorbent for Cu(II) removal from aqueous solutions.

3.4. Adsorption kinetics

In order to investigate the mechanism of adsorption kinetics, three widely used kinetic models Morris-Weber, pseudo-first-order and pseudo-second-order kinetic models have been investigated for their validity with the experimental adsorption data of Cu(II) onto FA. Studying the kinetic of Cu(II) adsorption onto ZA was impossible since the adsorption process attained an equilibrium state in a very short time. Many adsorption phenomena are dependent on time with different adsorbents.

The pseudo-first-order kinetic model of Lagergren assumes that the rate of change of solute uptake with time is proportional to the difference in the equilibrium adsorption capacity and the adsorbed amount at any time t . The linearized form of this kinetic model can be expressed as [46]:

$$\log(q_e - q_t) = \log q_e - \frac{k_1}{2.303} t \tag{6}$$

where k_1 (h^{-1}) is the first order rate constant; q_e and q_t (mg g^{-1}) are the amounts of Cu(II) adsorbed at equilibrium and at any time t , respectively.

The linear plot of $\log(q_e - q_t)$ versus t is shown in Fig. 7a. The rate constant (k_1) and the amount of Cu(II) adsorbed at equilibrium (q_e) can be calculated from the slope and intercept of the straight line, respectively. The calculated parameters as well as the correlation coefficient (R^2) are given in Table 3. As it is obvious, the experimental data is fitted with a relatively poor correlation factor, indicating that the pseudo-first-order kinetic model is not applicable to properly describe the Cu(II) adsorption onto FA.

The pseudo-second-order kinetic model is based on the adsorption capacity of the solid phase and it is in agreement with the chemisorption mechanism being the rate-limiting step [47]. The linear form of pseudo-second-order rate equation of Ho and McKay is expressed as [14]:

$$\frac{t}{q_t} = \frac{1}{k_2 q_e^2} + \frac{t}{q_e} \tag{7}$$

where k_2 ($\text{g mg}^{-1} \text{h}^{-1}$) is the pseudo-second-order adsorption rate constant. Fig. 7b illustrates the linear plot of t/q_t versus t . The values of k_2 and q_e calculated from the intercept and slope of the straight line and the correlation factor (R^2) are presented in Table 3. The results reveal that the adsorption process of Cu(II) onto FA well followed the pseudo-second-order kinetic model. In fact, the obtained experimental results support the assumption behind the kinetic model, suggesting that the rate controlling step in the adsorption process of Cu(II) onto FA is chemisorption mechanism which involves valence forces through sharing or exchanging electrons between the adsorbent and metal ions [48].

The pseudo-first-order and pseudo-second-order kinetic models are not able to explain the diffusion mechanism. For this purpose, the intra-particle diffusion model proposed by Weber and Morris was applied to analyze kinetic data. The intra-particle diffusion model is expressed as [14]:

$$q_t = K_{id} t^{0.5} + C \tag{8}$$

where k_{id} ($\text{mg g}^{-1} \text{h}^{-0.5}$) is the intra-particle diffusion rate constant and C (mg g^{-1}) is the intercept which gives information concerning the thickness of the boundary layer. If

Table 3
Kinetic parameters for Cu(II) adsorption onto FA

Kinetic model	Calculated Constants		
	k_1 (h^{-1})	q_e (mg g^{-1})	R^2
Pseudo-first-order	1.31	8.97	0.83
Pseudo-second-order	k_2 ($\text{g mg}^{-1} \text{h}^{-1}$)	q_e (mg g^{-1})	R^2
	0.27	8.71	0.99
Intra-particle diffusion	k_{id} ($\text{mg g}^{-1} \text{h}^{-0.5}$)	C (mg g^{-1})	R^2
	1.89	4.08	0.98

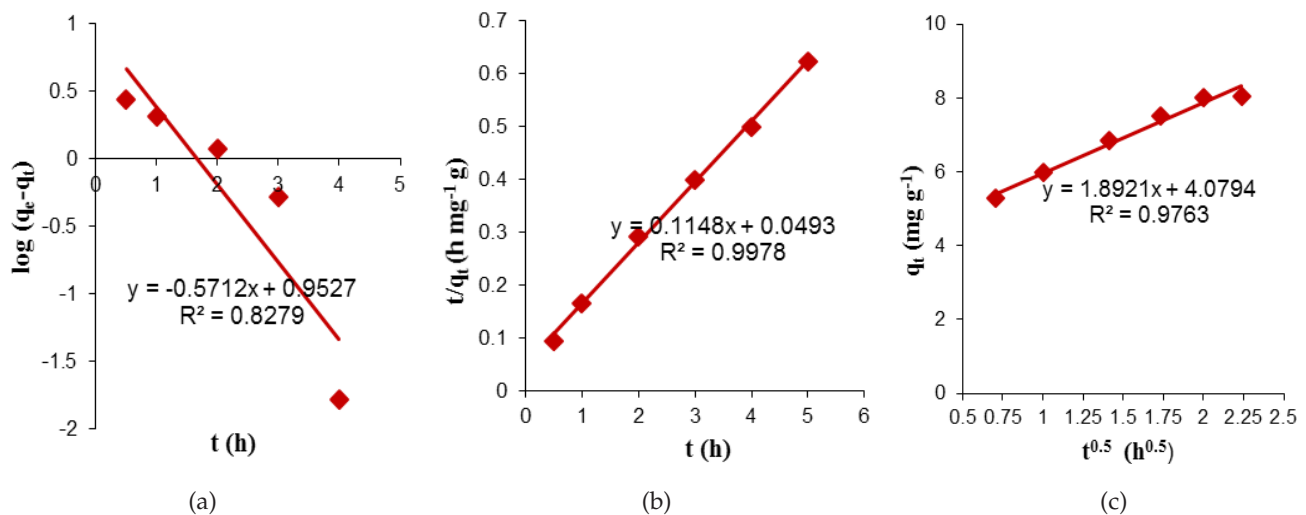


Fig. 7. Adsorption kinetic plots for Cu(II) adsorption onto FA: (a) Pseudo-first-order, (b) Pseudo-second-order, (c) Intra-particle.

the intra-particle diffusion is involved in the adsorption process, the plot of q_t against $t^{0.5}$ will be linear and if this line passes through the origin of the plot, the intra-particle diffusion is the sole rate-limiting step [49]. The first steep stage can be attributed to the diffusion of adsorbate through the solution to the external surface of the adsorbent or the boundary surface diffusion of the sorbate molecules. The second stage describes the gradual sorption, where intra-particle diffusion is rate-limiting, and the third stage is attributed to the final equilibrium due to extremely low sorbate concentration left in solution and the reduction of interior active sites [50].

The plot of q_t vs. $t^{0.5}$ is shown in Fig. 7c. The calculated amounts of intra-particle diffusion rate constant (k_{id}) and the intercept C as well as the correlation factor (R^2) are provided in Table 3. Furthermore, based on Fig. 7c, it is self-evident that the Cu(II) adsorption onto FA involves the intra-particle diffusion due to the linearity of the plot, although it is not the only rate-controlling step.

3.5. Effect of adsorbent dosage

Adsorbent dosage is an important parameter that is essential to be investigated in the adsorption processes because this parameter determines the capacity of an adsorbent for a given initial concentration of the adsorbate at the operating conditions [23]. The effect of FA and ZA dosages (0.05–0.4 g/50 mL solution) on the adsorption of Cu(II) ions (50 mg L^{-1}) was studied while the other operating parameters were constant. The results are presented in Fig. 8. As it can be observed, the adsorption percentage of Cu(II) onto FA and ZA increased with the increase of adsorbent dose, until it reached a maximum value of 96.2% around 0.3 grams of FA and it attained a saturation level of adsorption efficiency (97.5%) around 0.1 grams of ZA. These results may be attributed to the availability of more adsorption sites due to higher amounts of the adsorbent. At higher dosages, the equilibrium uptake of Cu(II) did not increase significantly with increasing of adsorbent. Such behavior is expected due to the saturation level attained during an adsorption process. As it is noticeable, less amounts (one-third) of adsorbent is required if ZA is utilized instead of FA for removing copper ions from aqueous solutions.

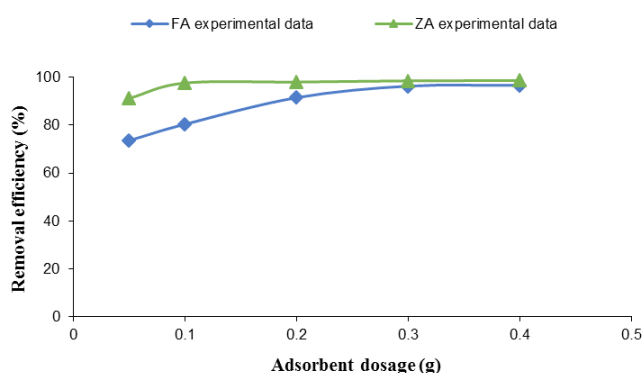


Fig. 8. Experimental data for adsorbent dosage effect on the removal efficiency of Cu(II) by FA and ZA.

3.6. Effect of initial metal ion concentration

The Cu(II) adsorption capacity of FA and ZA and the removal efficiency of metal ions as a function of initial Cu(II) concentration are shown in Fig. 9a,b. As it can be seen, the Cu(II) adsorption capacity of both FA and ZA firstly increased with increasing the initial concentration of metal ions until it attained a saturation value at around 200 ppm. The maximum equilibrium uptake of Cu(II) was about 16.6 mg g^{-1} for FA, while the maximum adsorption capacity of ZA was found to be 54.9 mg g^{-1} . Then the values did not significantly change with the initial metal ion concentration. Also, it is evident from the results that the percentage removal of copper ions decreased with increasing the initial concentration of metal ions for both cases. The reduction of Cu(II) adsorption may be attributed to the lack of available active sites required for the high initial concentration of copper ions. The higher uptake of copper ions at low concentration is due to the availability of more area on the surface of the adsorbent for less number of adsorbate species [33]. It can be concluded that ZA has higher adsorption capac-

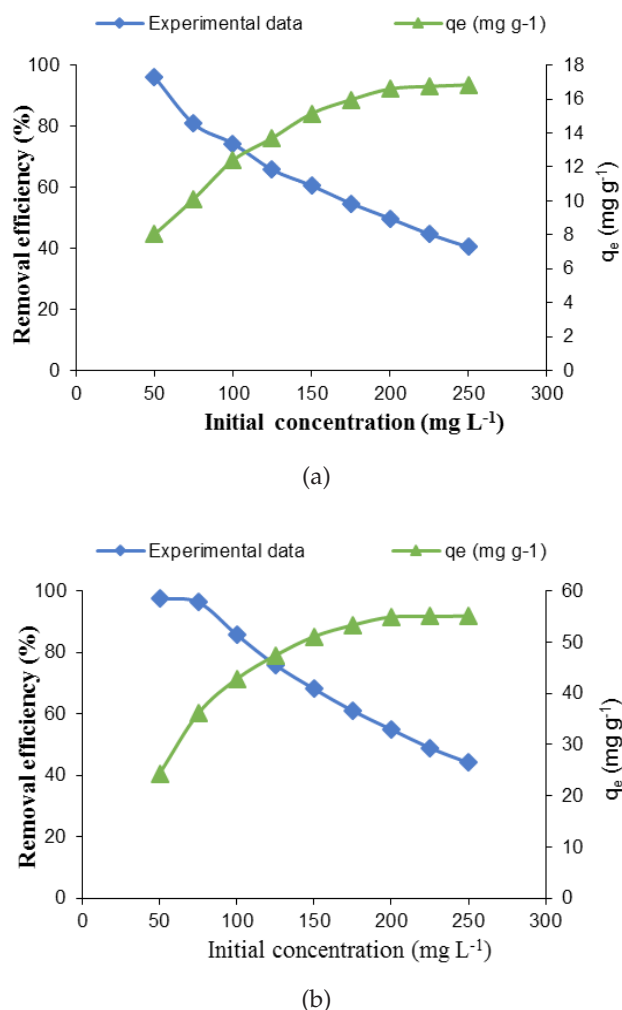


Fig. 9. The effect of initial concentration on the removal efficiency of Cu(II) by (a) FA and (b) ZA.

ities than FA; therefore, by using ZA as adsorbent more amounts of Cu(II) can be removed.

3.7. Adsorption isotherms

The adsorption isotherm model is based upon the hypothesis saying that all sorption sites are equivalent and their status does not depend on whether the neighboring sites are occupied or not [50]. Adsorption isotherm models generally represent the amount of adsorption at equilibrium as a function of equilibrium concentration at a constant temperature. The plots of q_e versus C_e for the adsorption of Cu(II) ions onto ZA and FA are presented in Fig. 10.

3.7.1. Langmuir isotherm model

The Langmuir isotherm model is based on the assumption that all the adsorption sites of the adsorbent are homogeneous and have identical adsorption energies and the maximum adsorption takes place when the adsorbent surface is covered by a saturated monolayer of solute molecules [8,51]. The linearized form of this isotherm model is expressed as follows:

$$\frac{C_e}{q_e} = \frac{1}{q_m K_L} + \frac{1}{q_m} C_e \quad (9)$$

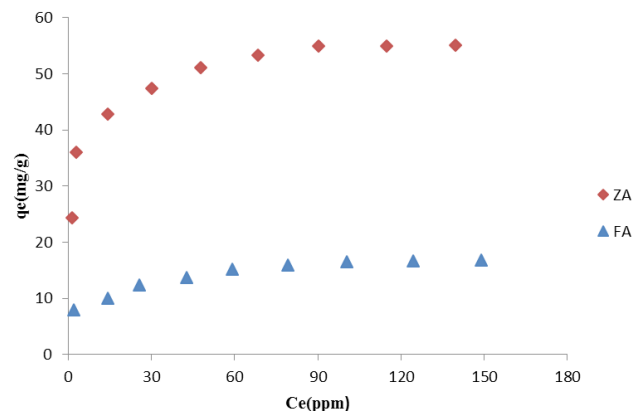


Fig. 10. Experimental adsorption isotherm as a plot of q_e vs. C_e .

Table 4
Isotherm parameters for Cu(II) adsorption onto FA and ZA

Langmuir equation	K_{L-ZA} (min ⁻¹)	K_{L-FA} (min ⁻¹)	q_{mZA} (mg/g)	q_{mFA} (mg/g)	R_{L-ZA}	R_{LFA}	R_{ZA}^2	R_{FA}^2
		0.29	0.11	56.49	17.82	0.013	0.035	0.99
Freundlich equation	K_{L-ZA} (min ⁻¹)	K_{L-FA} (min ⁻¹)	n_{ZA}	n_{FA}	R_{ZA}^2	R_{FA}^2		
	27.09	6.82	6.38	5.36	0.92	0.97		
Temkin equation	K_{T-ZA}	K_{T-FA}	B_{ZA}	B_{FA}	R_{ZA}^2	R_{FA}^2		
	67.69	12.15	6.22	2.25	0.97	0.94		
D-R equation	β_{ZA}	β_{FA}	q_{m-ZA}	q_{m-FA}	R_{ZA}^2	R_{FA}^2		
	4×10^{-7}	5×10^{-7}	50.65	14.54	0.88	0.59		

where q_e (mg g⁻¹) is the amount of metal ions adsorbed at equilibrium per specific amount of the adsorbent; C_e (mg L⁻¹) is the equilibrium metal ion concentration; q_m (mg g⁻¹) is the amount of metal ions adsorbed to form a monolayer, giving the maximum adsorption capacity of the adsorbent and K_L (L mg⁻¹) is the Langmuir constant.

The monolayer adsorption capacity, q_m , and the Langmuir constant, K_L , calculated from the slope and intercept of the linear plots as well as the related correlation factors, R^2 , are given in Table 4. As can be seen, Langmuir isotherm fits the experimental data very well which may be attributed to the homogenous distribution of active sites on the adsorbent surface, supporting the assumption behind the Langmuir isotherm model which considers the adsorption sites of the adsorbent as homogenous with the same adsorption energy.

The essential characteristics of Langmuir isotherm can be expressed in terms of a dimensionless constant separation factor, R_L , which is used to determine whether an adsorption system is favorable or unfavorable.

$$R_L = \frac{1}{1 + K_L C_0} \quad (10)$$

where K_L (L mg⁻¹) is the Langmuir constant and C_0 (mg L⁻¹) is the initial concentration of Cu(II). The value of R_L can indicate the shape of isotherm to be either unfavorable ($R_L > 1$) or linear ($R_L = 1$) or favorable ($0 < R_L < 1$) or irreversible ($R_L = 0$) [52]. The calculated amounts of R_L for Cu(II) adsorption onto FA and ZA which are given in Table 4 show that both raw fly ash and the zeolite prepared from it were favorable for the adsorption of Cu(II) from aqueous solution under the selected conditions.

3.7.2. Freundlich isotherm model

Freundlich equation is based on multilayer adsorption onto heterogeneous adsorbent surface with sites that have different adsorption energies. The linearized form of Freundlich equation can be shown as below [41,49]:

$$\log q_e = \log K_F + \frac{1}{n} \log C_e \quad (11)$$

where K_F is the Freundlich isotherm constant related to the relative adsorption capacity and n is a constant concerned with the intensity of adsorption.

The Freundlich constant, K_F and the value of constant n can be obtained from the intercept and slope of the linear plots, respectively. The magnitude of the exponent n gives information regarding the favorability of the adsorption process. It is generally said that the values of n in the range 2–10 indicate good, 1–2 moderately difficult and less than 1 poor adsorption characteristics [33]. The calculated amounts of K_F and n and the correlation coefficients (R^2) are summarized in Table 4. The results revealed that the adsorption processes of copper ions onto both FA and ZA are favorable with good adsorption characteristics.

3.7.3. Temkin isotherm model

The heat of adsorption and the interactions between adsorbents and adsorbates can be evaluated using Temkin isotherm model. Temkin isotherm model suggests that the reduction in the heat of adsorption is more linear rather than logarithmic as already expressed implicitly by the Freundlich equation. The linearized form of Temkin isotherm model is commonly described as [33]:

$$q_e = B \ln K_T + B \ln C_e \quad (12)$$

where $B = (RT/A_T)$ and the constant A_T (J mol^{-1}) is related to the heat of adsorption; T (K) is the absolute adsorption temperature; R ($8.314 \text{ J mol}^{-1} \text{ K}^{-1}$) is the universal gas constant and K_T (L min^{-1}) is the equilibrium binding constant corresponding to the maximum binding energy. The values of B and K_T can be obtained from the slope and intercept of the linear plots, respectively. Table 4 summarizes the results.

3.7.4. The Dubinin–Radushkevich isotherm model

To determine the nature of the sorption process namely chemisorption and/or physisorption, the Dubinin–Radushkevich (D–R) [53] isotherm was used. The linear form of this model is expressed by:

$$\ln(q_e) = \ln(q_m) - \beta \epsilon^2 \quad (13)$$

where q_e is the amount of Cu(II) adsorbed per unit dosage of the adsorbent (mg/g); q_m denotes the monolayer capacity; β indicates the activity coefficient related to the mean sorption energy and finally ϵ is the Polanyi potential described as:

$$\epsilon = RT \ln \left(1 + \frac{1}{C_e} \right) \quad (14)$$

The β , q_m values were determined by the slope and intercept of the linear plot using the plots of $\ln q_e$ versus ϵ^2 . Table 4 indicates the statistical results together with the isotherm constants. Results suggest that the Cu(II) sorption by ZA and FA can be matched using the Langmuir equation. Also, It can be understood from the D–R isotherm that the heterogeneity of energies is close to the adsorbent surface. The quantity is related to the mean sorption energy, E , which is the free energy for the transfer of 1 mole of Cu(II) from the infinity to the surface of the adsorbent [3,50]. The following equation shows how the mean free energy of adsorption (E , kJ/mol) is calculated [53,54]:

$$E = (2\beta)^{-0.5} \quad (15)$$

It is clear that we can use the E magnitude to estimate the adsorption type. If this value goes below 8 kJ/mol , the adsorption type is expressed by the physical sorption and between 8 and 16 kJ/mol the adsorption type can be explained by ion exchange. In this study, the E values were below 8 kJ/mol (1.18 and 1 kJ/mol for ZA and FA respectively). This reveals that the adsorption of Cu(II) onto ZA and FA was in fact a physical sorption [3,50].

3.8. Adsorption thermodynamics

3.8.1. Effect of temperature

Temperature is an important factor in adsorption processes which determines the nature of the adsorption with the calculation of thermodynamic parameters. The influence of temperature on the adsorption of Cu(II) onto FA and ZA was investigated at three different temperatures (25 , 35 and 45°C) as shown in Table 5. The removal efficiencies of FA and ZA for copper ions revealed an increase with rising temperature from 25 to 45°C . The increase in the amount of metal ions adsorbed onto the adsorbent surface with increasing temperature indicates the endothermic nature of the adsorption of Cu(II) ions onto FA and ZA. The increase in adsorption efficiency with temperature may be due to the increase in the number of active sites created because of breaking of some internal bonds near the edge of active sites of the adsorbent. This may also be attributed to the shrinkage of the boundary layer thickness surrounding the adsorbent, so that the mass transfer resistance of metal ions in the boundary layer reduces which results in an enhanced accessibility of the adsorbate molecules to the active sites of the adsorbent. Furthermore, the increase in the extent of adsorption with increasing temperature may stem from the strengthening of adsorptive forces between the active sites of adsorbents and the adsorbate species and between the neighboring molecules of the adsorbed phase [23,51].

3.8.2. Thermodynamics parameters

Thermodynamic parameters including the change in enthalpy (ΔH°), free energy (ΔG°) and entropy (ΔS°) were cal-

Table 5
The effect of temperature on the removal efficiency and thermodynamic parameters for Cu(II) adsorption onto FA and ZA

Adsorbent	T (K)	%Removal efficiency	ΔG° (kJ mol^{-1})	ΔH° (kJ mol^{-1})	ΔS° ($\text{kJ mol}^{-1} \text{ K}^{-1}$)
ZA	298.15	97.5	-7.34	+ 92.84	+ 0.33
	308.15	98.1	-8.36		
	318.15	99.7	-14.12		
FA	298.15	96.2	-3.59	+ 42.79	+ 0.15
	308.15	97.6	-4.90		
	318.15	98.7	-6.71		

culated using Eqs. (16)–(18) to explain the thermodynamic behavior of the adsorption of Cu(II) ions onto FA and ZA [45]:

$$K_D = \frac{q_e}{C_e} \tag{16}$$

$$\ln K_D = \frac{\Delta S^\circ}{R} - \frac{\Delta H^\circ}{RT} \tag{17}$$

$$\Delta G^\circ = -RT \ln K_D \tag{18}$$

where K_D is the thermodynamic equilibrium constant; R (8.314 J mol⁻¹ K⁻¹) describes the universal gas constant and T (K) is the absolute adsorption temperature. The values of ΔH° and ΔS° can be obtained from the slopes and intercepts of the linear plots of $\ln K_D$ versus 1/T by Eq. (17), respectively. The results are summarized in Table 5. As it can be observed, the values of ΔH° are both positive which confirm the endothermic nature of the adsorption processes. Furthermore, the reactions were accompanied by an increase in entropy. The positive values of ΔS° suggest an increase in the randomness at the adsorbent–adsorbate interfaces during the fixation of the ions on the adsorbent active sites. Moreover, the negative values of ΔG° indicate thermodynamically feasible and spontaneous nature of the adsorption processes.

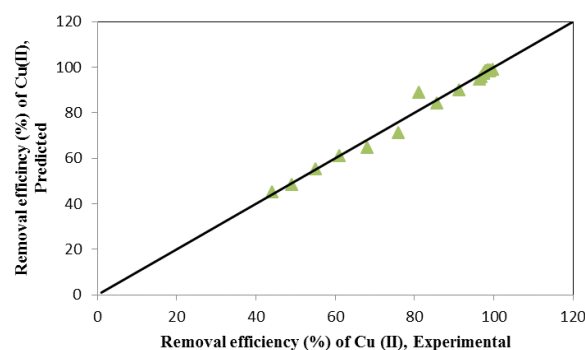
3.9. ANN modeling

Sola and Sevilla [55] represented that the effects of data normalization on the ANN process and concluded normalization of data yields better prediction, however, recently, it was reported that better results are yielded without normalization also [30–32]. In this study, all raw data are used as input variables without normalization. Table 6 indicates the input and output parameters used for ANN study along with the range of variables investigated. The total number of data points is 29. 70% (21), 15% (4) and 15% (4) data points were used for training, cross-validation and testing, respectively, for LM algorithms used. Fig. 11 indicates the comparison between the experimental and predicted data. It can be observed in Fig. 11 that the obtained results from the proposed ANN model are in excellent agreement with

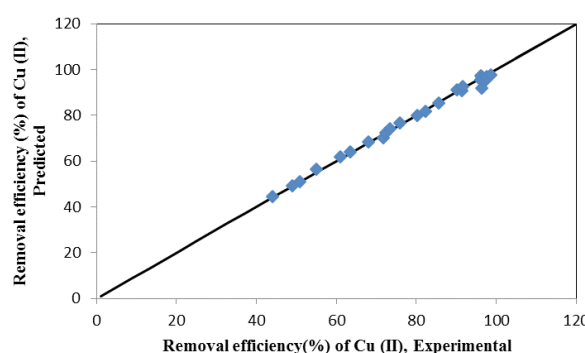
the data obtained from batch experiments of Cu(II) adsorption onto both FA and ZA.

3.10. Comparison of the Cu(II) maximum sorption capacity using various sorbents

To have a better understanding of the sorption capacity of ZA and FA, the values of the maximum removal obtained for Cu(II) ion uptake with various types of sorbents are indicated in Table 7. The experimental data collected from



(a)



(b)

Fig 11. Comparison between the experimental to the predicted removal efficiency (a) ZA (b) FA.

Table 6
Range of data for ANN modeling.

Input parameters	Range	Output parameters	Optimum number of hidden layers	Performance type	Transfer function	Number of input data	Number of output data
pH	2-6	Removal Efficiency	4	MSE	Logsig	29	29
Initial concentration	50–250ppm		6		Tansig		
Contact time (min)	0.5–6 h (FA), 5–60 min(ZA)		10		Linear		
Room temperature	25–45°C						
Adsorbent dosage	0.05–0.4 g						

Table 7
Comparison of the maximum sorption capacity (q_m) of the various sorbents

Sample	Sorbent material	q_m (mg/g)	Reference
1	ZA	56.49	This work
2	FA	17.82	This work
3	Humic acid-immobilized surfactant-modified zeolite	19.8	[56]
4	Chitosan-zeolite composite (CZ)	25.88	[47]
5	Acid-activated montmorillonite	32.3	[20]
6	Cellulose acetate/zeolite composite fiber	28.57	[14]
7	Nano-scale diboron trioxide/titanium dioxide (B_2O_3/TiO_2)	82	[57]
8	Iron-oxide nano-particles-immobilized sand (INS)	1.26	[58]
9	Cadmium Sulfide Nanoparticles	166.7	[59]

the present investigations are corresponding to the reported values. As shown in Table 7, the adsorption capacity of ZA is higher than Humic acid-immobilized surfactant-modified zeolite, Chitosan-zeolite composite (CZ), Acid-activated montmorillonite, Cellulose acetate/zeolite composite fiber and Iron-oxide nano-particles-immobilized sand (INS).

3.11. Desorption and regeneration studies

Regeneration of ZA and FA for reuse is crucial importance in industrial practice for Cu(II) sorption from aqueous solutions. Experiments were carried out for regenerating adsorbent to assess the reusability of ZA and FA for copper sorption. So, After the adsorption reached equilibrium (in optimum conditions), metal-loaded ZA and FA was separated from the mixture solution and then added into 50 mL of 0.1 M HCl solution for Cu(II) ion desorption. The contents of the flask were shaken at room temperature for 48 h, and the copper ion concentrations in the solution were analyzed. The adsorbent was finally separated from the solution. It was washed with distilled water and dried for reuse [18]. To indicate the reusability of the adsorbent, adsorption–desorption cycle of Cu(II) was repeated five times by the same preparations. The results are showed in Table 8, as can be seen, the removal efficiency has not changed considerable in the process of sorption–desorption, and the reduction of removal efficiency is less than 22% for both zeolite. Thus, the reuse of the soebent is an important feature for its possible application in continuous systems in industrial processes.

3.12. Adsorption mechanism

Based on the results obtained from sorption energy (E), physical sorption can be described as mechanism for the Cu(II) sorption on ZA and FA. Thus, Processes such as ion-

Table 8
Using the modified zeolite after regenerated

	Cu(II) removal efficiency (%)	
	ZA	FA
First time	97.8	96.3
Second time	90.5	87.35
Third time	85.14	82.34
Fourth time	82.21	78.3
Fifth time	79.4	74.85

exchange, chemical oxidation, and positively charged Cu(II) ions can form strong complexes interaction between Cu(II) ions and adsorbents surface. In addition, electrostatic interactions seem to be possible reactions which occur during heavy metal ions removal by oxygen-containing groups of ZA and FA. It can be concluded that Cu(II) sorption by ZA and FA is a complex process which several adsorption mechanisms including electrostatic attraction, ion exchange, and surface complexation play significant roles. However, due to the complex nature of sorption process, it is hard to determine the exact contribution of each sorption mechanism [60,61].

4. Conclusion

The present research revealed the efficiency of ZA as an attractive, low-cost adsorbent for the removal of Cu(II) from aqueous solutions. In comparison with FA ($q_e < 17 \text{ mg g}^{-1}$), higher adsorption capacities (up to $\sim 55 \text{ mg g}^{-1}$) could be achieved by using ZA as adsorbent for the removal of Cu(II) from aqueous solutions. Also, the Cu(II) adsorption onto ZA attained an equilibrium state after approximately 5 min, while the adsorption of copper ions by FA required more than 4 h to reach equilibrium. The optimum initial solution pH for Cu(II) adsorption onto both FA and ZA was determined to be 5, though ZA showed high adsorption efficiencies (96.8–98.9%) in a wide range of pH (3–6). The kinetics of Cu(II) adsorption onto FA followed Morris–Weber and pseudo-second-order equations as evident from the correlation coefficients. The study of Langmuir, Freundlich, Temkin, and D-R isotherm models showed that Cu(II) adsorption onto ZA and FA were both favorable with good adsorption characteristics. Meanwhile, the positive values of ΔH° (92.84 and 42.79 kJ mol^{-1}) and ΔS° (0.33 and 0.15 $\text{kJ mol}^{-1} \text{K}^{-1}$) for Cu(II) adsorption onto ZA and FA designated the endothermic nature of the adsorption processes as well as an increase in the randomness at adsorbent–adsorbate interfaces, whereas $-14.12 \text{ kJ mol}^{-1} < \Delta G^\circ < -7.34 \text{ kJ mol}^{-1}$ and $-6.71 \text{ kJ mol}^{-1} < \Delta G^\circ < -3.59 \text{ kJ mol}^{-1}$ for Cu(II) adsorption onto ZA and FA confirmed the feasibility and spontaneous nature of adsorption processes. The adsorption performances of FA and ZA in the treatment of Cu(II) from aqueous solutions were successfully predicted by applying a three-layer feed-forward MLP network using Levenberg-Marquardt back-propagation training algorithm. Different number of neurons in the hidden layer were tested and 6 neurons was found to have the best performance with the minimum MSE values of 6.1E-06 and 2.6E-05 for Cu(II) adsorption onto ZA and FA, respectively.

Acknowledgements

The work was supported by a grant from Tarbiat Modares University, Tehran, Iran. Meanwhile, we appreciate Maryam Bari, PhD student, Chemistry Dept., Simon Fraser University, Vancouver, Canada (Mbari@sfu.ca) for proof reading this article.

References

- [1] M. Visa, Synthesis and characterization of new zeolite materials obtained from fly ash for heavy metals removal in advanced wastewater treatment, *Powder Technol.*, 294 (2016) 338–347.
- [2] H. Pahlavanzadeh, A. Keshtkar, J. Safdari, Z. Abadi, Biosorption of nickel (II) from aqueous solution by brown algae: Equilibrium, dynamic and thermodynamic studies, *J. Hazard. Mater.*, 175 (2010) 304–310.
- [3] H. Esfandian, H. Javadian, M. Parvini, B. Khoshandam, R. Katal, Batch and column removal of copper by modified brown algae *Sargassum bevanom* from aqueous solution, *Asia-Pacific J. Chem. Eng.*, 8 (2013) 665–678.
- [4] I. Scheiber, R. Dringen, J.F. Mercer, Copper: effects of deficiency and overload. Interrelations between essential metal ions and human diseases, Springer, 2013, pp. 359–387.
- [5] F. Geyikçi, S. Çoruh, E. Kılıç, Development of experimental results by artificial neural network model for adsorption of Cu^{2+} using single wall carbon nanotubes, *Sep. Sci. Technol.*, 48 (2013) 1490–1499.
- [6] H. Cheng, Cu(II) Removal from lithium bromide refrigerant by chemical precipitation and electrocoagulation, *Sep. Purif. Technol.*, 52 (2006) 191–195.
- [7] N.G. Zaki, I. Khattab, N.A. El-Monem, Removal of some heavy metals by CKD leachate, *J. Hazard. Mater.*, 147 (2007) 21–27.
- [8] R. Katal, H. Pahlavanzadeh, Influence of different combinations of aluminum and iron electrode on electrocoagulation efficiency: Application to the treatment of paper mill wastewater, *Desalination*, 265 (2011) 199–205.
- [9] H. Ozaki, K. Sharma, W. Saktaywin, Performance of an ultra-low-pressure reverse osmosis membrane (ULPROM) for separating heavy metal: effects of interference parameters, *Desalination*, 144 (2002) 287–294.
- [10] L. Canet, M. Ilpide, P. Seta, Efficient facilitated transport of lead, cadmium, zinc, and silver across a flat-sheet-supported liquid membrane mediated by lasalocid A, *Sep. Sci. Technol.*, 37 (2002) 1851–1860.
- [11] X. Guo, S. Zhang, X.-q. Shan, Adsorption of metal ions on lignin, *J. Hazard. Mater.*, 151 (2008) 134–142.
- [12] S. Orlov, K. Burkov, M.Y. Skripkin, Adsorption of copper (II) ions from aqueous solutions on alumina industrial wastes, *Russ. J. Appl. Chem.*, 84 (2011) 2029–2032.
- [13] V.C. Dos Santos, J.V. De Souza, C.R. Tarley, J. Caetano, D.C. Dragunski, Copper ions adsorption from aqueous medium using the biosorbent sugarcane bagasse in natura and chemically modified, *Water, Air, Soil Pollut.*, 216 (2011) 351–359.
- [14] F. Ji, C. Li, B. Tang, J. Xu, G. Lu, P. Liu, Preparation of cellulose acetate/zeolite composite fiber and its adsorption behavior for heavy metal ions in aqueous solution, *Chem. Eng. J.*, 209 (2012) 325–333.
- [15] H.G. Roh, S.G. Kim, J. Jung, Adsorption of heavy-metal ions (Pb^{2+} , Cu^{2+}) on perm-lotion-treated human hair, *Korean J. Chem. Eng.*, 31 (2014) 310–314.
- [16] B. Singha, S.K. Das, Adsorptive removal of Cu(II) from aqueous solution and industrial effluent using natural/agricultural wastes, *Colloids Surfaces B: Biointerfaces*, 107 (2013) 97–106.
- [17] I. Cretescu, G. Soreanu, M. Harja, A low-cost sorbent for removal of copper ions from wastewaters based on sawdust/fly ash mixture, *Int. J. Environ. Sci. Technol.*, 12 (2015) 1799–1810.
- [18] M. Ahmad, A.R. Usman, S.S. Lee, S.-C. Kim, J.-H. Joo, J.E. Yang, Y.S. Ok, Eggshell and coral wastes as low cost sorbents for the removal of Pb^{2+} , Cd^{2+} and Cu^{2+} from aqueous solutions, *J. Ind. Eng. Chem.*, 18 (2012) 198–204.
- [19] C. Jeon, Adsorption characteristics of waste crab shells for silver ions in industrial wastewater, *Korean J. Chem. Eng.*, 31 (2014) 446–451.
- [20] K.G. Bhattacharyya, S.S. Gupta, Removal of Cu(II) by natural and acid-activated clays: An insight of adsorption isotherm, kinetic and thermodynamics, *Desalination*, 272 (2011) 66–75.
- [21] K.G. Bhattacharyya, S.S. Gupta, Removal of Cu(II) by natural and acid-activated clays: An insight of adsorption isotherm, kinetic and thermodynamics, *Desalination*, 272 (2011) 66–75.
- [22] R. Katal, E. Hasani, M. Farnam, M.S. Baei, M.A. Ghayyem, Charcoal ash as an adsorbent for Ni(II) adsorption and its application for wastewater treatment, *J. Chem. Eng. Data*, 57 (2012) 374–383.
- [23] M.J. Amiri, J. Abedi-Koupai, S.S. Eslamian, M. Arshadi, Adsorption of Pb (II) and Hg (II) ions from aqueous single metal solutions by using surfactant-modified ostrich bone waste, *Desal. Water Treat.*, 57 (2016) 16522–16539.
- [24] F. Fotovat, H. Kazemian, M. Kazemini, Synthesis of Na-A and faujasitic zeolites from high silicon fly ash, *Mater. Res. Bull.*, 44 (2009) 913–917.
- [25] M. Visa, L. Isac, A. Duta, Fly ash adsorbents for multi-cation wastewater treatment, *Appl. Surf. Sci.*, 258 (2012) 6345–6352.
- [26] J.d.C. Izidoro, D.A. Fungaro, J.E. Abbott, S. Wang, Synthesis of zeolites X and A from fly ashes for cadmium and zinc removal from aqueous solutions in single and binary ion systems, *Fuel*, 103 (2013) 827–834.
- [27] N.G. Turan, B. Mesci, O. Ozgonenel, The use of artificial neural networks (ANN) for modeling of adsorption of Cu(II) from industrial leachate by pumice, *Chem. Eng. J.*, 171 (2011) 1091–1097.
- [28] M. Dutta, P. Ghosh, J.K. Basu, Application of artificial neural network for the decolorization of direct blue 86 by using microwave assisted activated carbon, *J. Taiwan Inst. Chem. Eng.*, 43 (2012) 879–888.
- [29] U. Yurtsever, M. Yurtsever, I.A. Şengil, N. Kıratlı Yılmazçoban, Fast artificial neural network (FANN) modeling of Cd(II) ions removal by valonia resin, *Desal. Water Treat.*, 56 (2015) 83–96.
- [30] S. Nag, A. Mondal, N. Bar, S.K. Das, Biosorption of chromium (VI) from aqueous solutions and ANN modelling, *Environ. Sci. Pollut. Res.*, 24 (2017) 18817–18835.
- [31] B. Singha, N. Bar, S.K. Das, The use of artificial neural network (ANN) for modeling of Pb (II) adsorption in batch process, *J. Molec. Liq.*, 211 (2015) 228–232.
- [32] B. Singha, N. Bar, S.K. Das, The use of artificial neural networks (ANN) for modeling of adsorption of Cr (VI) ions, *Desal. Water Treat.*, 52 (2014) 415–425.
- [33] S.H. Asl, M. Ahmadi, M. Ghiasvand, A. Tardast, R. Katal, Artificial neural network (ANN) approach for modeling of Cr (VI) adsorption from aqueous solution by zeolite prepared from raw fly ash (ZFA), *J. Ind. Eng. Chem.*, 19 (2013) 1044–1055.
- [34] P. Davoodi, S.M. Ghoreishi, A. Hedayati, Optimization of supercritical extraction of galegine from *Galega officinalis* L.: Neural network modeling and experimental optimization via response surface methodology, *Korean J. Chem. Eng.*, (2015) 1–12.
- [35] S. Ghoreishi, A. Hedayati, S. Mousavi, Quercetin extraction from *Rosa damascena* Mill via supercritical CO_2 : Neural network and adaptive neuro fuzzy interface system modeling and response surface optimization, *J. Supercrit. Fluids*, 112 (2016) 57–66.
- [36] A. Hedayati, S. Ghoreishi, Artificial neural network and adaptive neuro-fuzzy interface system modeling of supercritical CO_2 extraction of glycyrrhizic acid from *Glycyrrhiza glabra* L., *Chem. Prod. Process Model*, 11 (2016) 217–230.
- [37] D. Kamar, Fly ash-coal combustion residue, EBS 425/3–Mineral Perindustrian, (2009).
- [38] J.d.C. Izidoro, D.A. Fungaro, F.S. dos Santos, S. Wang, Characteristics of Brazilian coal fly ashes and their synthesized zeolites, *Fuel Process. Technol.*, 97 (2012) 38–44.

- [39] M. Harja, G. Buema, D.M. Sutiman, C. Munteanu, D. Bucur, Low cost adsorbents obtained from ash for copper removal, *Korean J. Chem. Eng.*, 29 (2012) 1735–1744.
- [40] C.-F. Wang, J.-S. Li, L.-J. Wang, X.-Y. Sun, Influence of NaOH concentrations on synthesis of pure-form zeolite A from fly ash using two-stage method, *J. Hazard. Mater.*, 155 (2008) 58–64.
- [41] H. Pahlavanzadeh, R. Katal, H. Mohammadi, Synthesize of polypyrrole nanocomposite and its application for nitrate removal from aqueous solution, *J. Ind. Eng. Chem.*, 18 (2012) 948–956.
- [42] A.A. Babaei, A. Khataee, E. Ahmadpour, M. Sheydaei, B. Kaka-vandi, Z. Alaee, Optimization of cationic dye adsorption on activated spent tea: Equilibrium, kinetics, thermodynamic and artificial neural network modeling, *Korean J. Chem. Eng.*, 33 (2016) 1352–1361.
- [43] M. Šljivić, I. Smičiklas, S. Pejanović, I. Plečaš, Comparative study of Cu^{2+} adsorption on a zeolite, a clay and a diatomite from Serbia, *Appl. Clay Sci.*, 43 (2009) 33–40.
- [44] B. Al-Rashdi, C. Tizaoui, N. Hilal, Copper removal from aqueous solutions using nano-scale diboron trioxide/titanium dioxide ($\text{B}_2\text{O}_3/\text{TiO}_2$) adsorbent, *Chem. Eng. J.*, 183 (2012) 294–302.
- [45] F. Zhao, Y. Zou, X. Lv, H. Liang, Q. Jia, W. Ning, Synthesis of CoFe_2O_4 -zeolite materials and application to the adsorption of gallium and indium, *J. Chem. Eng. Data*, 60 (2015) 1338–1344.
- [46] L. Zhai, Z. Bai, Y. Zhu, B. Wang, W. Luo, Fabrication of chitosan microspheres for efficient adsorption of methyl orange, *Chinese J. Chem. Eng.*, 26 (2017) 657–666.
- [47] W.W. Ngah, L. Teong, R. Toh, M. Hanafiah, Utilization of chitosan-zeolite composite in the removal of Cu(II) from aqueous solution: adsorption, desorption and fixed bed column studies, *Chem. Eng. J.*, 209 (2012) 46–53.
- [48] R. Katal, H. Zare, Abouzar fani, Mohamad Omraei, G.D. Najaf-pour, Removal of zinc from aqueous phase by charcoal ash, *World Appl. Sci. J.*, 13 (2011) 331–340.
- [49] J. Lin, Y. Zhan, Z. Zhu, Adsorption characteristics of copper (II) ions from aqueous solution onto humic acid-immobilized surfactant-modified zeolite, *Colloids Surf. A: Physicochem. Eng. Asp.*, 384 (2011) 9–16.
- [50] H. Esfandian, A. Samadi-Maybodi, M. Parvini, B. Khoshan-dam, Development of a novel method for the removal of diazinon pesticide from aqueous solution and modeling by artificial neural networks (ANN), *J. Ind. Eng. Chem.*, 35 (2016) 295–308.
- [51] A. Adamczuk, D. Kołodyńska, Equilibrium, thermodynamic and kinetic studies on removal of chromium, copper, zinc and arsenic from aqueous solutions onto fly ash coated by chitosan, *Chem. Eng. J.*, 274 (2015) 200–212.
- [52] S. Wong, N.A.N. Yac'cob, N. Ngadi, O. Hassan, I.M. Inuwa, From pollutant to solution of wastewater pollution: synthesis of activated carbon from textile sludge for dyes adsorption, *Chinese J. Chem. Eng.*, 26 (2017) 870–878.
- [53] M.M. Dubinin, L. Radushkevich, Equation of the characteristic curve of activated charcoal, *Chem. Zentr*, 1 (1947) 875.
- [54] T. Naiya, A. Bhattacharya, S. Das, Removal of Cd (II) from aqueous solutions using clarified sludge, *J. Colloid Interf. Sci.*, 325 (2008) 48–56.
- [55] J. Sola, J. Sevilla, Importance of input data normalization for the application of neural networks to complex industrial problems, *IEEE Trans. Nucl. Sci.*, 44 (1997) 1464–1468.
- [56] R.M. Aghav, S. Kumar, S.N. Mukherjee, Artificial neural network modeling in competitive adsorption of phenol and resorcinol from water environment using some carbonaceous adsorbents, *J. Hazard. Mater.*, 188 (2011) 67–77.
- [57] B. Al-Rashdi, C. Tizaoui, N. Hilal, Copper removal from aqueous solutions using nano-scale diboron trioxide/titanium dioxide ($\text{B}_2\text{O}_3/\text{TiO}_2$) adsorbent, *Chem. Eng. J.*, 183 (2012) 294–302.
- [58] S.-M. Lee, C. Laldawngliana, D. Tiwari, Iron oxide nano-particles-immobilized-sand material in the treatment of Cu(II), Cd(II) and Pb(II) contaminated waste waters, *Chem. Eng. J.*, 195–196 (2012) 103–111.
- [59] S. Golkhah, M.H. Zavvar, H. Shirkanloo, A. Khaligh, Removal of ions from aqueous solutions by cadmium sulfide nanoparticles, *Int. J. Nanosci. Nanotechnol.*, 13 (2017) 105–117.
- [60] L. Hui, D.-l. Xiao, H. Hua, L. Rui, P.-l. Zuo, Adsorption behavior and adsorption mechanism of Cu(II) ions on amino-functionalized magnetic nanoparticles, *Trans. Nonferr. Metals Soc. China*, 23 (2013) 2657–2665.
- [61] S.I. Lyubchik, A.I. Lyubchik, O.L. Galushko, L.P. Tikhonova, J. Vital, I.M. Fonseca, S.B. Lyubchik, Kinetics and thermodynamics of the Cr (III) adsorption on the activated carbon from co-mingled wastes, *Colloids Surf. A: Physicochem. Eng. Asp.*, 242 (2004) 151–158.